Predicting sample lifetimes in creep fracture of heterogeneous materials

Juha Koivisto, Markus Ovaska, Amandine Miksic, Lasse Laurson, and Mikko J. Alava
COMP Centre of Excellence, Department of Applied Physics, Aalto University, P. O. Box 11100, FIN-00076, Aalto, Espoo, Finland
(Received 21 September 2015; published 8 August 2016)

Materials flow—under creep or constant loads—and, finally, fail. The prediction of sample lifetimes is an important and highly challenging problem because of the inherently heterogeneous nature of most materials that results in large sample-to-sample lifetime fluctuations, even under the same conditions. We study creep deformation of paper sheets as one heterogeneous material and thus show how to predict lifetimes of individual samples by exploiting the "universal" features in the sample-inherent creep curves, particularly the passage to an accelerating creep rate. Using simulations of a viscoelastic fiber bundle model, we illustrate how deformation localization controls the shape of the creep curve and thus the degree of lifetime predictability.

DOI: 10.1103/PhysRevE.94.023002

I. INTRODUCTION

The problem of how to predict material strength and sample failure is where engineering, materials science, and physics meet [1–4]. The predictability of lifetimes of structures and materials involves phenomena on various scales, beginning with atomic interactions. In brittle fracture, sample failure is governed by statistical strength laws: by dividing a material sample into independent subvolumes [5], its strength is determined by the statistics of extremes [6,7] or, in essence, by the spirit of the renormalization group [5]. One may know the probability distribution of the failure stresses *a priori* but no more.

In contrast to brittle materials, most real materials are often ductile to some degree and exhibit a complicated rheological creep response under constant applied loads [8–11]. To simplify the typical time-dependent creep response to constant applied loads that lead to failure, we can divide it into primary, secondary, and tertiary creep [12,13]: initial strain-hardening (described by the Andrade law) [14,15], steady-state or logarithmic creep [16], and a final phase in which the strain rate ϵ_t increases, implying strain softening [17], finally leading to sample failure. For the paper samples we study here, this progression is illustrated in Fig. 1, which shows a typical creep strain versus time behavior and experimental details. The figure also illustrates the use of digital image correlation (DIC) in such experiments to obtain strain fields and strain rate fields at different stages of creep.

As a direct, consequential result of such a sequence of events, *for any sample*, two characteristic time scales are evident: the sample lifetime t_c and the time t_m, at which the creep rate versus time curve $\epsilon_t(t)$ exhibits a minimum [lower inset of Fig. 2(a)]. Beyond t_m, the sample strain rate accelerates towards final failure. For heterogeneous materials, the creep curves, and thus both of these time scales (t_m and t_c), may exhibit large sample-to-sample fluctuations, even for experiments performed under identical conditions (applied load, temperature, humidity, etc.).

Here we consider the possibility of exploiting correlations between t_m and t_c (and other properties of the creep curves of individual samples) to predict their lifetimes [8,18–20]. To this end, we first discuss the typical sample-dependent properties of the creep strain rate curves $\epsilon_t(t)$. Then, we study various lifetime prediction schemes, taking advantage of the curves' regularities from sample to sample, including the relative location in time t_m/t_c of the minimum creep rate. We show that it is possible to predict lifetimes of individual samples with a heterogeneous microstructure since there is a strong correlation between t_c and t_m. By performing numerical simulations of viscoelastic fiber bundle models, we show that the regularities in the time-dependent creep deformation process underlying such predictability are related to geometry-controlled deformation localization, an effect that precedes the final failure of the sample. Finally, we summarize the results.

II. EXPERIMENTS

We performed constant load creep experiments on ordinary copy paper, a quasi-two-dimensional material, using an Instron Electropuls E1000 tensile testing machine, see Fig. 1(a). Since the mechanical properties of paper depend on temperature and humidity [21,22], the tests were performed under constant conditions (23°C, rH 50%) in a controlled testing chamber. The default sample size is 50 × 100 × 0.1 mm (width × height × thickness); the applied load was chosen so that the majority of the samples (for which largest statistics have been collected to measure the sample-to-sample fluctuations under identical loads) have typical lifetimes of 20 min maximum (see also the Supplemental Material (SM), Fig. S7 [23]). The constant load is reached by a linear load ramp lasting 5 s (see SM, Fig. S1, for the impact of this on the measurement of short lifetimes t_c; SM and Fig. S4, also contain discussion of more complicated stop-and-go loading protocols). Simultaneous acoustic emission (AE) measurements showed that only very few AE events could be detected, at least prior to close to t_c.

The material characteristics of the paper sheets are the grammage (areal weight) $\rho_g = 80$ g/m^2, breaking threshold $P_b = 24$ MPa (2.4 kN/m; typical tensile index for cross-direction copy paper is 20–40, breaking threshold $P_b =$ 1.6–3.2 kN/m), and Young's modulus $E = 2.2$ GPa. The internal displacement sensor of the testing machine produces the global engineering strain $\epsilon = (l - l_0)/l_0$ (with l and l_0 the actual and initial length of the sample, respectively). In addition, we can calculate displacements in an evenly spaced grid, with a typical grid spacing of 1 mm, by simultaneously using the DIC method [Fig. 2(b)] [24,25]. The local strain is defined as $\epsilon_{loc} = (uy_{i,j+1} - uy_{i,j})/\mathrm{dist}(r_{i,j}, r_{i,j+1})$, where

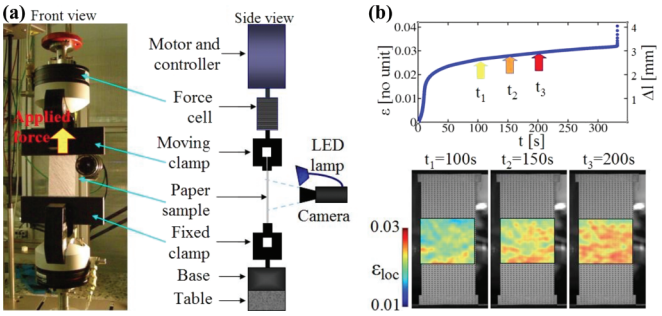

FIG. 1. Experimental setup to study the spatiotemporal creep dynamics of paper samples. (a) The tensile testing machine where the paper sample, attached between two clamps, is subject to a constant applied force. (b) A typical creep curve and example strain maps computed by digital image correlation analysis for three times t_1, t_2, and t_3, showing how the strain fluctuations develop towards the localization of deformation leading finally to sample failure.

uy is the primary displacement parallel to loading (j and y coordinate) and r is the position vector.

A. Scaling of creep properties

By performing a large set of creep experiments under different conditions, we can establish a linear relation $t_m \propto at_c$ [17], with a a constant (for more detail, including the variety of experiments performed, see the SM). We find $a = 0.83 \pm 0.01$ [26] and a wide range of t_cs spanning three orders of magnitude [Fig. 2(a); see also SM, Figs. S1, S2, and S5]. Generally and depending on the material, the constant a attains values that reflect the typical shape of the creep curve and, in particular, it is often much smaller than 0.83 (see Refs. [27,28] for examples). This behavior is reminiscent to what is known in materials science as the Monkman-Grant (MG) relation [29], where t_c is often correlated with the minimum strain rate, $\epsilon_{t,\min}$ [30]. The MG relation is usually used in the context of variations in the experimental conditions (load, temperature, etc.) causing the subsequent variations in t_c [18,31,32]. Here we consider the relation correlating t_c with t_m [rather than with $\epsilon_{t,\min} \equiv \epsilon_t(t_m)$] in the context of the sample-to-sample variability that arises from the heterogeneous nature of the material.

A general ansatz for the sample and time-dependent creep rate [8] would be $\epsilon_t(t) = \epsilon_{t,\min} f(t/t_c)$, if the sample-dependent shape of the creep curve can be summarized by the lifetime and minimum creep rate only. Figure 2(a), upper inset, shows that the parts of the different creep curves corresponding to the two last regimes—logarithmic (where $\epsilon_t \sim t^{-1}$) and tertiary—can indeed be collapsed onto a single master curve using such an ansatz. Doing so also reveals a divergence of ϵ_t as t_c is approached, $\epsilon_t \propto (t_c - t)^{-b}$, with $b \approx 1.0$ [9,33] (see also SM, Fig. S6). This behavior suggests the possibility to predict the sample lifetime t_c, exploiting the "universal" properties of the creep curve, implied by the data collapse.

B. Predicting t_c

Clearly, we should use the measured value of t_m for a sample to predict its t_c, via the relation $t_c = t_m/a$ [19,20]. Finding

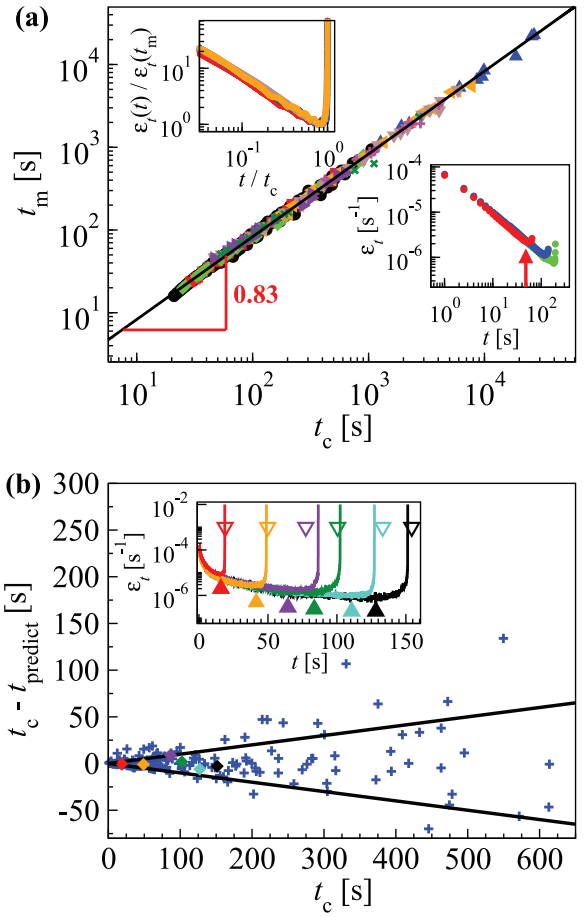

FIG. 2. (a) The time of the minimum creep rate t_m as a function the sample lifetime t_c for a large number of experiments, including different loading conditions and sample geometries, and also repeating the experiment several times using the same conditions. The data are well described by $t_m = 0.83\ t_c$. Lower inset: Time dependence of strain rate ϵ_t for three example experiments, all exhibiting a minimum strain rate at time $t = t_m$ (shown with a red arrow in one case) before acceleration towards final failure at time $t = t_c$. Upper inset: A data collapse of six creep curves after rescaling the time axis by the lifetime t_c and the vertical axis by the minimum strain rate $\epsilon_t(t_m)$ [9]. (b) Comparisons of lifetime predictions (t_c) to the actual values of lifetime, t_c, with the black lines corresponding to a 10% difference between the predicted and actual value of t_c. Inset: Six different cases of actual prediction experiments. The full symbols correspond to minimum strain rate time t_m estimates and the open ones to the corresponding t_c predictions. The ϵ_t data are shown with the curves. The six cases are also marked in the main figure with the correspondingly colored symbols.

t_m from the data—*a posteriori* or during an experiment—is somewhat complicated for two reasons: experimental noise and intrinsic fluctuations [24,26] in the instantaneous sample creep rate [see Fig. 3(a) for an example $\epsilon_t(t)$ curve]. In other words, the sample creep rate varies in time so even though the envelope curve for $\epsilon_t(t)$ is easy to establish, on smaller time scales, both measurement accuracy and actual creep rate fluctuations become important.

The slow decay of ϵ_t when approaching t_m implies that estimating t_m during the experiment by approximating—as

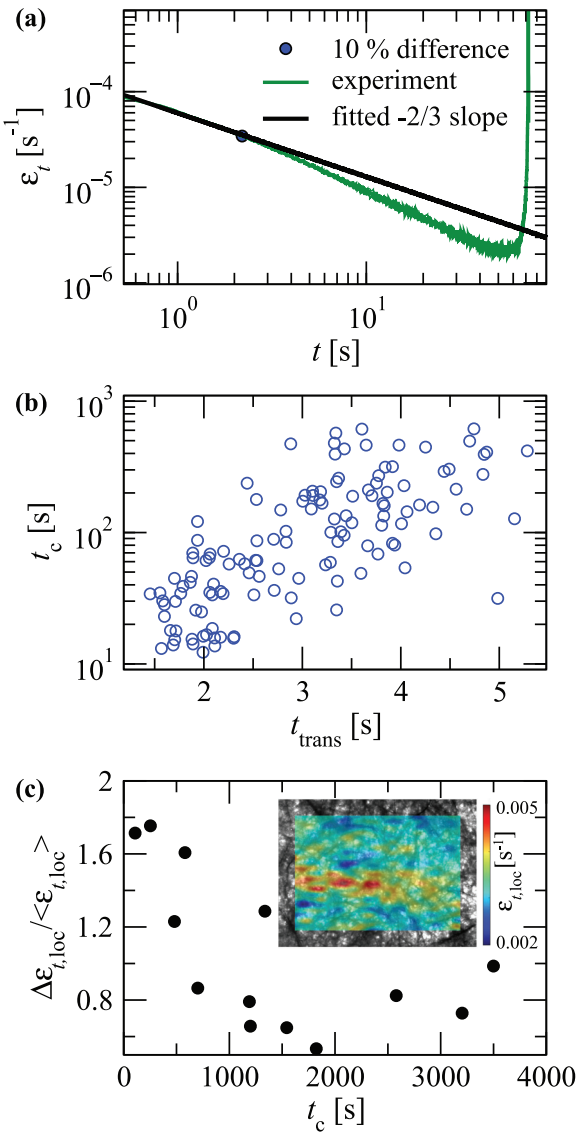

FIG. 3. (a) Definition of the transient time t_{trans} corresponding to the crossover from primary to secondary creep regime is here given by the point (blue dot) at which a fit (black line) corresponding to the typical Andrade or primary creep law, $\epsilon_t = At^{-2/3}$, deviates more than 10% from the data (shown in green). (b) t_c as a function of the corresponding t_{trans}, revealing a roughly exponential trend, $\langle t_c(t_{trans})\rangle \sim \exp(t_{trans}/t_0)$. (c) Shows that the relative spatial strain rate fluctuations, computed by DIC 128 s from the start of the experiment using a time window of 10 s (see the inset for an example of a map of the fluctuating local strain rates), exhibit an inverse correlation with the lifetime, t_c.

a trial approach—ϵ_t in the neighbourhood of $t = t_m$ with a second-order polynomial is difficult. Thus, we chose the simple method to fit a straight line to the $\epsilon_t(t)$ data within time intervals of length Δt (chosen here as 10 s, see the SM for more details). Then, we define t_m as the time at which the slope of the fitted line changes sign. In other words, we compute the moving average of the strain rate over Δt and search for the zero of the time derivative. Figure 2(b) shows how this approach works. Typically, we can reach an accuracy of 10% of the t_c prediction. The inset of Fig. 2(b) shows how this works in a few particular cases: the t_m estimated and the t_c computed from the estimate. Sample-to-sample fluctuations in the t_m determination from the experimental ϵ_t data, as well as from the natural variations around the average MG-like relation, produce errors in the prediction scheme; the SM contains an analysis of the magnitude of the expected error.

One may ask if t_c can be predicted by considering signatures [18] observable already at earlier stages of creep (i.e., for $t < t_m$, see also SM for more discussion). The secondary creep sample-dependent details of the creep curve are not useful for lifetime prediction as no noticeable correlation exists between the slope A of the creep rate in the logarithmic phase [20], where $\epsilon_t \propto At^{-1}$, and both t_m and t_c. In Fig. 3(a) and 3(b), we consider the correlation between the time of the crossover from primary (Andrade) to secondary (logarithmic) creep, t_{trans}, with t_c (recall that the whole creep curve does not permit a collapse). Figure 3(b) shows that this crossover implies a correlation and thus a degree of predictability, with a roughly exponential trend $\langle t_c(t_{trans})\rangle \sim \exp(t_{trans}/t_0)$. However, this effect is much less useful for prediction than the relation between t_m and t_c, given the large fluctuations of t_c for a given t_{trans}. One can also consider the sample-dependent spatial strain [24] (as those shown in Fig. 1) or strain rate fluctuations [26] [Fig. 3(c)] obtained by DIC [24,34] during the early stages of the creep process. The data in Fig. 3(c) indicate that samples with large relative strain rate fluctuations $\Delta\epsilon_{t,loc}/\langle\epsilon_{t,loc}\rangle$ (standard deviation of local rates normalized by the mean rate), reflecting the presence of heterogeneities in the sample material structure, tend to break earlier than samples with small fluctuations [24]. Again, this approach has only limited predictive power, as implied by large fluctuations of t_c for a given $\Delta\epsilon_{t,loc}/\langle\epsilon_{t,loc}\rangle$.

III. LOCALIZATION OF DEFORMATION AND LIFETIME DISTRIBUTIONS

Geometry-controlled deformation localization may cause the transition at $t = t_m$ from strain hardening to softening. We next show how to understand this using a viscoelastic serial fiber bundle model (SFBM) [5,35,36]. The SFBM exhibits an early strain-hardening material response, thus mimicking the slowing creep rate (primary or secondary types of creep). It thus catches as a model the salient features of creep experiments but is not intended to have more than descriptive power, e.g., as regards the influence of material microstruture on creep behavior. As it is a discrete model of fibers or elements it assumes the implicit presence of a material-dependent length scale, which is relevant for the damage or strain localization the model exhibits [5,24]. Analogous to the loading geometry of the creep experiments, the fiber bundle layers (of which there are N_s, with N_p fibers each) carry load in series, each having a random failure threshold, allowing for an eventual localization of deformation to a single layer. We simulate viscoelastic SFBMs with a fixed total number of fibers, $N = N_p \times N_s = 256\,000$, for various N_s, each with viscoelastic constitutive behavior [5,35]. That behavior is modeled by a Kelvin-Voigt element [35], or the constitutive equation $\sigma_0 = \beta\epsilon_t + E\epsilon$ of the fibers, with β a damping constant, E the Young modulus, and σ_0 the constant external load (here we set $\beta = E = 1$ for simplicity). In addition to such viscoelastic

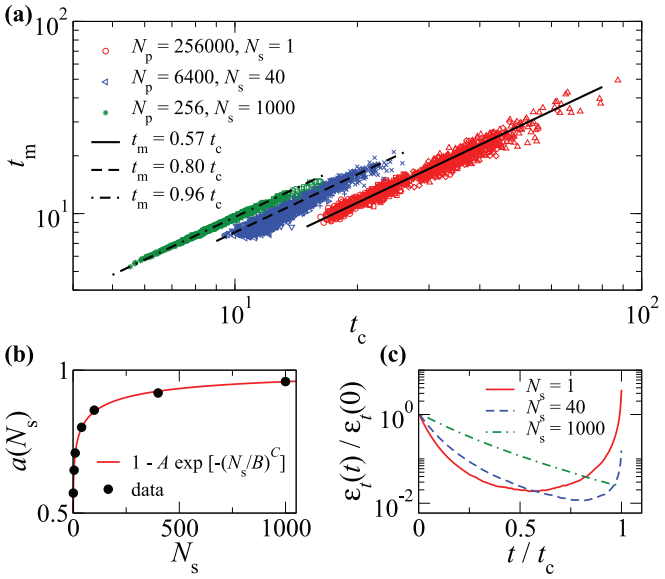

FIG. 4. (a) The MG $[t_m(t_c)]$ relation is depicted for three different geometries of the viscoelastic SFBM, i.e., different values of the number N_s of bundles connected in series. For each N_s (with $N_s = 1$, 40, and 1000 shown in red, blue, and green, respectively), we consider also several load values (shown with different symbols) close to but above the critical load required to break the sample. (b) The evolution of $t_m/t_c \equiv a(N_s)$ with N_s. The solid line corresponds to a fit of the form of $a(N_s) = 1 - Ae^{-(N_s/B)^C}$, with $A = 0.69 \pm 0.01$, $B = 17.6 \pm 0.1$, and $C = 0.26 \pm 0.01$. (c) Examples of the scaled creep curves for the three N_s values shown in (a). Notice how the minimun strain rate time t_m moves towards the lifetime t_c as N_s is increased.

dynamics, we include a failure criterion for the fibers, implying that a fiber fails if its strain exceeds a local and random failure threshold ϵ_c with a probability density $p(\epsilon_c)$. In the simulations, we choose $p(\epsilon_c)$ to be a uniform distribution between 0 and 1; other bounded distributions yield similar results. If a fiber fails, then the load is equally distributed among the remaining intact fibers within the bundle (global load sharing) [5]. Thus, the time evolution of the individual fiber bundles (of which there are N_s in series) is described by $\sigma_0/[1 - P(\epsilon)] = \beta\epsilon_t + E\epsilon$, where P is the cumulative distribution of the failure thresholds [35]. The time-dependent deformation behavior of each of the N_s FBMs in series is computed by numerical integration of this equation. The global rheology of the serial model is obtained as a sum over the N_s independent subsystems, and the rheology, analogous to creep experiments, exhibits an initial deformation stage with a decreasing creep rate, followed by accelerating deformation towards its final failure. The small N_s limit of this model is known to lead to a roughly parabolic creep curve and to fix t_m/t_c to 0.5. Obviously, this limit could be varied by tuning the rheology of the model.

For applied loads close to but above the critical value required to eventually break the sample, we observe a linear relation $t_m = a(N_s)t_c$, with a somewhat smaller range of t_cs than in our experiments [Fig. 4(a)]. Such a relation can be used to predict the sample lifetimes if we measure t_m from the data before failure. As shown in Fig. 4(b), the slope $a(N_s)$ varies

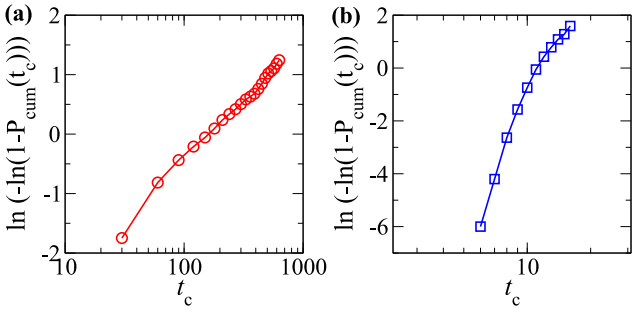

FIG. 5. Lifetime histograms shown for the experiments (a) and the model (b) using a "Weibull paper" [plotting the inverse cumulative lifetime distribution $1 - P_{cum}(t_c)$ using a double logarithmic scale].

with N_s, from close to 0.5 ($N_s = 1$) towards 1 with $N_s \to \infty$. Figure 4(c) shows examples of the creep curves for different values of N_s. This behavior as a function of N_s is a consequence of the extremal statistical nature of the problem: The weakest layer will eventually control the sample approach to failure, leading to geometry-dependent deformation behavior [7].

Thus, in the spirit of extremal statistics arguments where such functional forms are often encountered, we compare the $a(N_s)$ data with a stretched exponential, $a(N_s) = 1 - Ae^{-(N_s/B)^C}$, and obtain a reasonable fit with $A = 0.69 \pm 0.01$, $B = 17.6 \pm 0.1$, and $C = 0.26 \pm 0.01$. This kind of weak dependence of a on N_s means that experimentally testing this scaling prediction by varying the sample dimensions is difficult. The model implies that sample-to-sample variations (the disorder of each sample) dictate the crossover from strain-stiffening to localization and strain-softening (tertiary creep; see also SM, Fig. S8). This crossover yields a linear relation between t_m and t_c, with a geometry-dependent prefactor controlling t_m, and thus determines how early during the creep process the sample lifetime can be predicted.

One important aspect is the lifetime distribution of the samples, which can be obtained from both the experimental data and the model. Figure 5(a) presents the histogram of t_cs for a set of 170 nominally identical samples from experiments performed under identical conditions. It compares experimental data with the serial fiber bundle model using three different geometries (as above, $N_s = 1$, 40, and 1000, with $N = 256\,000$). The empirical histogram seems to be wider and exhibits a tail towards long lifetimes (SM, Fig. S3), which appears to be power-law-like with an exponent close to -1. We next test whether the experiments or the model could be captured with a "weakest link" or extremal statistics analysis. In this scope, Fig. 5(a) shows the experimental data plot in a way that would reveal if the histogram follows a two-parameter Weibull distribution. A linear behavior cannot be established (a Weibull exponent fit shows a very small exponent value of about 0.8, which should not be meaningful), and the statistics obtained from the model simulations are even less Weibull-like. Thus, the lifetime distributions do not follow weakest link scenarios of brittle time-dependent failure, in which the system failure takes place when the weakest subsystem reaches its lifetime [37–39]. This is not a surprise in the SFBM because it exhibits a more complex rheology than models of brittle fracture do. The causality implied by

the model is such that the t_m that signals the transition to the deformation localization determines t_c, not vice versa, and t_m does not follow from weakest-link-like arguments.

The final question we address relates to the predictability of the *location* of the nucleation of the final crack leading to the eventual failure of the paper sample: Do the local yielding dynamics [2] correlate prior to t_m with the final localization or where the crack will be? This, however, is found not to be the case: The "activity spots" [40] detected by DIC during the early stages of creep are not significantly correlated with the final deformation localization and sample failure. In the experiments (material) at hand, typical fluctuations have a fairly large spatial scale compared to the sample size [24,26]. Also, the final crack is detectable using infrared thermography [41] only roughly 1 s before the sample failure (SM, Figs. S9 and S10).

IV. SUMMARY

We have studied in depth the sample-to-sample variations in creep fracture of paper samples—an example of a heterogeneous material—and explored the possibility of forecasting the sample lifetime and the location where the sample fails using modeling and experiment. We found that the linear t_m vs t_c relation can be used to predict t_c of individual samples of paper. This predictability is particularly important in the sample-to-sample variability under equal testing conditions; it also extends to other loads and more complicated loading protocols. For the current test case, our approach is able to predict roughly the last 20% of the sample lifetime, which—as conjectured by the model—is a material and loading-geometry-dependent quantity. For other materials/cases, the "83%" is expected to assume other values, typically smaller ones.

This is an early "warning signal" rather than a final divergence of the creep rate (see Fig. 2) as the sample-dependent t_c is approached. Other research considers two related, bordering cases: the subcritical dynamics of single cracks [42,43] and using acoustic emission (AE) as a diagnostic for failure prediction, analogous to the tertiary creep strain rate divergence results shown in Fig. 2 [18,33,44–47]. The current work differs in two general and major ways: We examine samples without (or prior to the formation of) a dominating crack, before the moment the dynamics of such a crack dictates the remaining lifetime, and when there is no degree of AE that could be used as a signal for failure.

We have discovered earlier signatures of the creep deformation process that correlate with the eventual t_c, shown in Fig. 3. In addition, predicting the actual location of the final crack is an intrinsically hard task. To elaborate, there are two issues: deciphering from local strain rate fields $\epsilon_{t,\mathrm{loc}}$ where the creep deformation will be localized during the transition to tertiary creep and when that will take place (t_m). Early correlations imply memory effects: The sample lifetime is correlated with the "sample quality" to a degree. The fields $\epsilon_{t,\mathrm{loc}}$ are used to see this by choosing a suitable time interval inside which the magnitudes of these local deformation rates correlate with the time-dependent strength, or the sample lifetime. The question now is this: Can we find better measures for lifetime prediction than to correlate t_m with t_c? Our results imply that, prior to t_m, ϵ_t itself does not have any useful, hidden properties. DIC provides the $\epsilon_{t,\mathrm{loc}}$ information. The fields are reasonably detailed in time (with time intervals of small fractions of the duration of any particular experiment) and spatially limited to the accuracy reachable by DIC (subpixel strains). There are three obvious candidates for quantities that could be studied for predictability: fluctuations (see above), early signs of the final localization of deformation in tertiary creep and in crack formation, and the identification of larger than average local yielding ("slip events"). After some trials, none of these seems viable.

To reproduce the relation between t_m and t_c, we present a simple model of localization, reproducing the $t_c(t_m)$ relation, and predicting that it, and, consequently, the possibility to predict sample lifetimes, depends on the sample geometry. The deterministic features (e.g., t_m) do not result from "critical phenomena," but the final temporal increase of the strain rate and its functional dependence (on $t_c - t$) could arise from collective deformation processes. The physics of the model also agrees with our empirical lack of success in finding schemes for t_c prediction that would apply earlier than t_m. Thus, we have found that predictability of creep fracture incorporates several issues: intrinsic material rheological behavior, the fluctuations that follow from the randomness or disorder in the material, and the sample geometry that is most relevant for the deformation localization and for the degree of lifetime predictability.

ACKNOWLEDGMENTS

We acknowledge the financial support of the Academy of Finland through an Academy Research Fellowship (L.L., Project No. 268302) and the Finnish Centres of Excellence Program (Project No. 251748).

[1] D. Sornette, Proc. Natl. Acad. Sci. USA **99**, 2522 (2002).
[2] E. D. Cubuk, S. S. Schoenholz, J. M. Rieser, B. D. Malone, J. Rottler, D. J. Durian, E. Kaxiras, and A. J. Liu, Phys. Rev. Lett. **114**, 108001 (2015).
[3] T. H. Dixon *et al.*, Proc. Natl. Acad. Sci. USA **111**, 17039 (2014).
[4] G. F. Nataf *et al.*, J. Phys.: Condens. Matter **26**, 275401 (2014).
[5] M. J. Alava, P. Nukala, and S. Zapperi, Adv. Phys. **55**, 349 (2006).
[6] E. J. Gumbel, *Statistics of Extremes* (Columbia University Press, New York, 2004).
[7] C. Manzato, A. Shekhawat, P. K. V. V. Nukala, M. J. Alava, J. P. Sethna, and S. Zapperi, Phys. Rev. Lett. **108**, 065504 (2012).
[8] B. Voight, Science **243**, 200 (1989).
[9] M. Leocmach, C. Perge, T. Divoux and S. Manneville, Phys. Rev. Lett. **113**, 038303 (2014).
[10] J. Lin, E. Lerner, A. Rosso, and M. Wyart, Proc. Natl. Acad. Sci. USA **111**, 14382 (2014).

[11] A. Lemaitre, Phys. Rev. Lett. **113**, 245702 (2014).
[12] R. N. Nabarro and F. De. Villiers, *Physics of Creep and Creep-Resistant Alloys* (Taylor & Francis, London, 1995).
[13] I. G. Main, Geophys. J. Int. **142**, 151 (2000).
[14] E. N. da C. Andrade, Proc. R. Soc. A **84**, 1 (1910).
[15] F. Louchet and P. Duval, Int. J. Mat. Res. **100**, 1433 (2009).
[16] A. H. Cottrell, Philos. Mag. Lett. **75**, 301 (1997).
[17] H. Nechad, A. Helmstetter, R. El Guerjouma, and D. Sornette, Phys. Rev. Lett. **94**, 045501 (2005).
[18] A. Guarino, S. Ciliberto, A. Garcimartín, M. Zei, and R. Scorretti, Eur. Phys. J. B **26**, 141 (2002).
[19] J. M. Alegre, I. I. Cuesta, and M. Lorenzo, Exp. Mech. **54**, 1441 (2014).
[20] S.-W. Hao, B.-J. Zhang, J.-F. Tian, and D. Elsworth, J. Geophys. Res. **119**, 1942 (2014).
[21] H. W. Haslach, Mech. Time. Dep. Mat. **4**, 169 (2000).
[22] M. J. Alava and K. J. Niskanen, Rep. Prog. Phys. **69**, 669 (2006).
[23] See Supplemental Material at http://link.aps.org/supplemental/10.1103/PhysRevE.94.023002 for additional details of the experiments and simulations.
[24] A. Miksic, J. Koivisto, and M. J. Alava, J. Stat. Mech. (2011) P05002.
[25] J. Kybic and M. Unser, IEEE Trans. Im. Proc. **12**, 1427 (2003).
[26] J. Rosti, J. Koivisto, L. Laurson, and M. J. Alava, Phys. Rev. Lett. **105**, 100601 (2010).
[27] M. S. Gopala Krishna, A. M. Sriramamurthy, and V. M. Radhakrishnan, J. Mater. Eng. Perform. **7**, 548 (1998).
[28] T. Sakthivel, S. Panneer Selvi, and K. Laha, Mater. Sci. Eng. A **640**, 61 (2015).
[29] F. C. Monkman and N. J. Grant, ASTM Spec. Tech. Publi. **56**, 593 (1956).
[30] F. Povolo, J. Mater. Sci. **20**, 2005 (1985).
[31] D. C. Dunand, B. Q. Han, and A. M. Jansen, Metal. Mat. Trans. A **30**, 829 (1999).
[32] H. O. Ali and M. N. Tamin, J. Nucl. Mater. **433**, 74 (2013).
[33] J. Vasseur *et al.* Sci. Rep. **5**, 13259 (2015).
[34] F. Hild and S. Roux, Strain **42**, 69 (2006).
[35] R. C. Hidalgo, F. Kun, and H. J. Herrmann, Phys. Rev. E **65**, 032502 (2002).
[36] F. Kun, R. C. Hidalgo, H. J. Herrmann, and K. F. Pal, Phys. Rev. E **67**, 061802 (2003).
[37] S. Mahesh and S. L. Phoenix, Int. J. Fract. **127**, 303 (2004).
[38] Z. P. Bazant, J.-L. Le, and M. Z. Bazant, Proc. Natl. Acad. Sci. USA **106**, 11484 (2009).
[39] A. Mattsson and T. Uesaka, Phys. Rev. E **92**, 042158 (2015).
[40] A. Amon, V. B. Nguyen, A. Bruand, J. Crassous, and E. Clement, Phys. Rev. Lett. **108**, 135502 (2012).
[41] R. Toussaint, O. Lengliné, S. Santucci, T. Vincent-Dospital, M. Naert-Guillot, and K. J. Måløy, Soft Matter **12**, 5563 (2016).
[42] S. Santucci, L. Vanel, and S. Ciliberto, Phys. Rev. Lett. **93**, 095505 (2004).
[43] S. Santucci, P.-P. Cortet, S. Deschanel, L. Vanel, and S. Ciliberto, Europhys. Lett. **74**, 595 (2006).
[44] J.-C. Anifrani, C. Le Floc'h, D. Sornette, and B. Souillard, J. Phys. I France **5**, 631 (1995).
[45] A. Bell, J. Greenhough, M. J. Hap, and I. G. Main, Geophys. J. Int. **185**, 718 (2011).
[46] A. F. Bell, M. Naylor, M. J. Heap, and I. G. Main, Geophys. Res. Lett. **38**, L15304 (2011).
[47] S. Lennartz-Sassinek, I. G. Main, M. Zaiser, and C. C. Graham, Phys. Rev. E **90**, 052401 (2014).